Article N° 541
Contribution C.O.B. N° 732

OCEANOLOGICA ACTA 1981 - VOL. 4 - N° 4

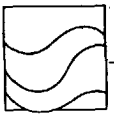

Bottom currents
Deep-sea sediments
Texture
Magnetic fabric
Paleocirculation

Courants de fonds
Sédiments profonds
Granulométrie
Propriétés magnétiques
Paléocirculation

Deep-sea sediments texture and magnetic fabric, indicators of bottom currents regime

G.-A. Auffret [a], B. Sichler [a], B. Coléno [b]

[a] Centre Océanologique de Bretagne, BP n° 337, 29273 Brest Cedex.

[b] Groupe d'Intérêt Scientifique n° 9, Océanologie et Géodynamique, CNRS-CNEXO-UBO, Université de Bretagne Occidentale, avenue Victor Le Gorgeu, 29283 Brest Cedex.

Received 15/1/81, in revised form 13/5/81, accepted 21/5/81.

ABSTRACT

Critical speeds for erosion, transport and deposition of sedimentary particles and prevailing bottom currents intensities are in such a range that the textural properties of the sediment silt fraction may be correlated to the intensity of the deep circulation. On the other hand, the long axis of the sediment magnetic susceptibility ellipsoid, should be aligned according to the current flow.

These hypotheses have been positively tested in five abyssal areas. The authors then apply textural studies to the study of Cenozoic deep water circulation in two continental margin areas (Bay of Biscay and Western Mediterranean, DSDP Site 400 and Site 372). The results are in good agreement with informations provided by micropaleontological and geochemical indicators.

Oceanol. Acta, 1981, **4**, 4, 475-488.

RÉSUMÉ

Texture et fabrique magnétique des sédiments abyssaux, indicateurs du régime des courants de fonds.

Les conditions d'érosion, de transport et de dépôt des particules sédimentaires et la gamme des vitesses des courants de fond susceptibles de prévaloir en milieu abyssal sont telles que les propriétés texturales de la fraction silteuse des sédiments paraissent pouvoir être corrélées à l'intensité de la circulation profonde. D'autre part, le grand axe de l'ellipsoïde des indices de susceptibilité magnétique des sédiments paraît s'aligner selon la direction du courant prévalant à l'interface.

Un test de ces hypothèses dans cinq secteurs de la zone abyssale apparaît positif. Les auteurs appliquent la première de ces techniques (texture) à l'étude de l'évolution de la circulation profonde au cours du Tertiaire dans deux sites des marges continentales (golfe de Gascogne et Méditerranée occidentale, DSDP sites 400 et 372). L'évolution mise en évidence est en accord avec les informations fournies par les indicateurs géochimiques et micropaléontologiques.

Oceanol. Acta, 1981, **4**, 4, 475-488.

INTRODUCTION

Can deep-sea surface sediments be considered as natural long term current meter? If so, then a new tool for the study of the present deep-sea circulation will be at our disposal, and furthermore, the sedimentary record could then be considered as a potential paleocurrent-meter using actualistic or uniformitarian principles. We present in this paper:

1) the theoretical background of a model that aims to predict hydrodynamic parameters in the bottom

boundary layer from the texture and magnetic fabric of surface sediments;
2) a test of the model in five areas from the Atlantic Ocean and the Mediterranean Sea;
3) an attempt to reconstruct paleocirculation from two Cenozoic sequences.

THEORETICAL BACKGROUND

Current intensity

Attempts to interpret textural parameters of sediments, in terms of their hydrodynamic significance, have been particularly numerous for near-shore environments, but the amount of work devoted to deep-sea deposits is far less abundant (Oser, 1972; Gonthier, Klingebiel, 1973; Van Andel, 1973; McCave, Swift, 1976; Grousset, 1977; Huang, Watkins, 1977; Stow, Lovell, 1979; Craig, 1979). The broad spectrum of sedimentary processes in deep sea environments, difficulty in analytical techniques, together with financial costs are three possible reasons for this. However, the importance of sediment reworking by normal oceanic currents has recently received greater recognition due to increased interest in deep-sea sediment processes through applied research projects.

In Table 1, we have summarized the different sedimentary processes that may operate in the deep-sea and the related deposits. These could be broadly classified into two categories. In the first group (gravity control), the energy is provided by the force of gravity acting on the material being transported. In the second group, energy is supplied by a "normal" oceanic current, i.e. those currents resulting from the action of external agents (geostrophic, wind driven, tidal, inertial, ...) on water masses. As we want to point to the relation between sedimentary deposits and "normal" oceanic currents, it is necessary to be able to assess from the deposit, which type of sedimentary processes it originates from. Criteria for the distinction between muddy turbidites and contourites may be found in Stow and Lovell (1979).

Table 2
Criteria for the recognition of muddy contourites.
Critères pour la reconnaissance des contourites vaseuses.

Criterion	Characteristics of muddy contourites after Stow and Lovell (1979)
Physiographic setting	Continental slope and rise, marginal plateau, sediment ridge.
Sedimentation rates	Generally lower than 10 cm/1 000 years.
Sedimentary structures	Dominantly homogeneous and bioturbated.
Sedimentary fabric	Small randomly arranged particles clusters. Grain orientations parallel to the current (along slope).
Texture	Dominantly silty, with sand content lower than 15%.
Mineralogy	Biogenic and terrigenous components. In interbedded coarse lag deposits the nature of the biogenic sand fraction is similar to that of the homogeneous mud one.

Lithological sections suitable for paleocirculation studies, could be recognized according to the criteria summarized in Table 2.

Figure 1 after Hollister and Heezen (1972), gives for each particle size the critical velocities for erosion, transport and deposition. We have plotted on this diagram the distribution in percent of the maximum bottom current velocities recorded in different areas of the world oceans (Auffret, Pastouret, 1975; Auffret *et al.*, 1975 and unpublished data, Stow, Lovell, 1979; Barusseau, Vanney, 1978). This histogram indicates that silt-sized particles (between 8 and 63 μm) could be eroded and/or transported in most areas. However, average sands (200 μm) are too coarse to be eroded, and average "clay particles" (3 μm) are, depending on their cohesion state, either "never deposited" or "never eroded". Medium silts (averaging 23 μm according to our choice) are eroded for a current velocity of 6 cm . sec.$^{-1}$ and transported until the velocity decreases under 0,5 cm . sec.$^{-1}$. Thus the hydrodynamic properties of the silt fraction make it a sensitive indicator of the bottom current velocities prevailing in the deep ocean.

Table 1
Classification of deep sea deposits in relation with the sedimentary processes responsible for their deposition.
Classification des dépôts de mer profonde et processus sédimentaires responsables de leur mise en place.

Control	Sedimentary processes	Lifting agent	Deposits	References
Gravity flow or current	Debris flow	Matrix	Conglomerate and breccia	Kuenen (1950-1967), Kuenen and Migliorini (1950), Walker (1973), Mutti and Ricci-Lucchi (1972), Middleton Hampton (1976)
	Sand flow	Dispersive pressure	Fluxoturbidite; Resedimented conglomerate	
	Fluidized flow	Intergranular flux	Sandy turbidite	
	Turbidity current: High concentration; Low concentration: Spill over, Thick, Thin	Turbulence of the water-sediment mixture	Silty clayey turbidity	Nelson *et al.* (1977); Gennesseaux *et al.* (1971), Keller *et al.* (1973), Shepard *et al.* (1977), Stow and Bowen (1978), Moore (1969).
Oceanic current	Density current (cascading); Bottom current: Strong (20 cm/sec.), Weak (1 to 20 cm/sec)	Vertical component of sea-water turbulence	"Cascadite"; Sandy contourites; Silty-clayey contourites	Nelson *et al.* (1973); Heezen and Hollister (1964), Hollister and Heezen (1972), Eittreim and Ewing (1972), Stow and Lovell (1979)
Gravity	Vertical settling		Hemipelagite; Pelagite	Arrhenius (1963), Berger (1974)

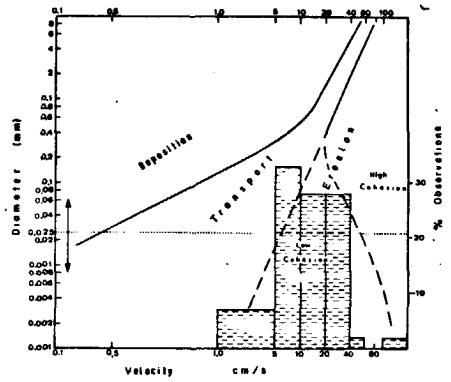

Figure 1

Critical velocities for erosion, transport and deposition, and percentage distribution of the maximum bottom current velocities recorded in different areas of the world ocean.

Vitesse critique pour l'érosion, le transport et le dépôt des particules sédimentaires avec distribution en pourcentage des vitesses maximales de courant de fond enregistrées dans diverses zones océaniques.

However, the reported values of velocities imply that the sediment texture is relatively homogeneous. In the case of mixture, the finer particles could be preserved as a result of a sheltering effect.

According to McCave and Swift (1976) the rate of deposition R_d of a given particle size is expressed by a relationship involving the ratio of the actual shear to the critical shear:

$$R_d = \rho_d \times N_d \times U_d \times P'(1 - T \times T_{cd}^{-1}),$$

ρ_d, particle density; U_d, particle settling velocity; N_d, particle concentration; T, shear stress at the water sediment interface; T_{cd}, critical shear stress for erosion of particle size "d"; P', probability factor accounting for local influence $1 > P' > 0$.

Following this relationship the proportion of the silt fraction coarser or finer than average silt size (23 μm) is a function of the local shear.

The deposited material is commonly subjected to mixing processes related to bioturbation in the benthic layer (Rowe, 1974). The thickness of the mixed layer (6 to 18 cm according to Peng *et al.*, 1977), and the rate of turnover are such that the material, once deposited and buried, is periodically reexposed to the action of bottom currents. The time increment D_t, during which a particle may be exposed to the bottom current action is:

$$D_t = D \times R^{-1},$$

D, depth of the mixed layer; R, rate of accumulation.

For D ranging from 6 to 18 cm and R from 1 to 10 cm/1 000 y D_t may range from 600 y to 18 000 y.

The periods are still short relative to the Cenozoic and Pleistocene time scale, but are long compared to the Holocene one (0 to 10 000 BP). From the above observation, we postulate that the median size of the sediment silt fraction can provide information about sedimentary processes occurring at the bottom boundary layer. The coarser the silt median, the stronger the stress exerted by the bottom current on the sea floor. Moreover if the distribution of the particles in the silt fraction is current-controlled, the median of the carbonate and non-carbonate (residual) fractions should be positively correlated. And if a positive correlation exists, this indicated hydrodynamic current control, for there is no *a priori* reason for such a correlation, for particles of different sedimentary origin, such as foraminifer tests or debris, fine quartz debris and biogenous siliceous remains. We therefore interpret high values of the median sizes and high correlation coefficients as indicative of high energy levels at the bottom boundary layer.

The comparison of textural parameters of different grain types within a sediment in order to infer the importance of the hydrodynamic control, has already been used for continental shelf sand (Barusseau, 1973) and deep sea sediments (Diester-Haass, 1973; 1975).

However, one may argue that dissolution of carbonate and siliceous microfossils may bias the median size of the silt fractions, and therefore lead to misinterpretation. Based on observations of biological reworking in pelagic sediments referenced above, it is evident that both dissolution and hydrodynamic sorting operate simultaneously during the time period D_t.

Thus, it may be postulated (if we admit that no further dissolution operates below the mixed zone), that the dissolution effect does not hinder the hydrodynamic particle size control. Another consequence of McCave and Swift's formula is that the sedimentation rate should be inversely correlated with the intensity of the stress exerted by bottom currents on the sea floor, the extreme case being the absence of sedimentation which would result in a hiatus in the geological record.

As a result of the above hypothesis, we propose to use the hydrodynamic indices listed below:

1) for surface sediments devoid of carbonate:

$$C_1 = M_{ds}^2 \times (23^2)^{-1} \times 100;$$

2) for marly surface sediments:

$$C_2 = M_{dsr} \times M_{dsc} \times (23^2)^{-1} \times 100;$$

3) for population of marly surface sediments:

$$C_3 = \overline{M}_{dsr} \times \overline{M}_{dsc} \times (23^2)^{-1} \times r \times 100.$$

M_{ds}, silt median; M_{dsr}, non-carbonate silt fraction median; M_{dsc}, carbonate silt fraction median; r, correlation coefficient; 23 μm, average silt.

$\overline{M}_{dsr}$ and $\overline{M}_{dsc}$ are the average median grain sizes of silt fractions from surface sediments sampled in a particular area of the ocean floor.

According to the chosen silt-size range (8-63 μm), the hydrodynamic indice C_3 may theoretically range between −750 and +750.

C_1 and C_2 indices are characteristic of individual samples. They allow a direct comparison of sediment samples according to their hydrodynamic "level". The

calculation of indice C_3 implies that we may consider a set of samples from a given area of the sea-floor as part of a statistic population. Therefore, we calculate an hydrodynamic indice (applying to a sea-floor area), in which enters the correlation coefficient (r) between the median size of the non-carbonate and carbonate silt fractions of surface sediment samples pertaining to this specific area.

Current direction

No quantitative theory as to the orientation of grains in unidirectional flow has as yet been formulated. However, work by Rusnak (1957), Hamilton (1967), Rees (1968), and Hamilton and Rees (1970) demonstrate that elongate grains of silt-size range are predominantly deposited with the long axis orientated parallel to flow direction. This can be shown using simple physical principles. As a result of the shear velocities that may be encountered at abyssal depths, particle deposition occurs in a laminar layer, approximately one millimeter thick. In this laminar layer, elongate particles are orientated in such a way that they offer as little resistance as possible to friction, implying that grain orientation will be parallel to current streak (McCave, Swift, 1976). Thus this orientation is most likely to be adopted by elongate particles once they have been deposited. Experimental data obtained from silt-sized material demonstrate particularly well this phenomenon (Hamilton, 1967). Bioturbation processes within the mixed layer, may totally destroy this hydrodynamically-induced fabric. However, as will be discussed later, fabric destruction is only partial.

On the basis of depositional behavior two kinds of magnetic grains can be identified:

1) grains larger than 10 μm which are deposited with their long axes parallel to current flow; and

2) smaller grains, which are orientated by the local magnetic field, due to a sheltering effect.

This difference in depositional behavior has two significant results:

1) the magnetic susceptibility of sediment (Fig. 2) is characterized by an ellipsoid, the long axis of which is parallel to the current direction and the short axis is orientated at an angle $\hat{\alpha}$ that ranges between 50 and 90° relatively to the horizontal;

2) the direction of north can be obtained from the remanent magnetism, which is related to the orientation of the smaller mono-domain magnetic particles.

From the above information the azimuth of the flow direction can be calculated. Several parameters have been proposed to characterize sedimentary magnetic fabric (Rees, 1965): lineation (L), foliation (F), anisotropy percentage (h), and q such as:

$$L = K_{max} - K_{int};$$

$$F = (K_{max} + K_{int}) \times 2^{-1} - K_{min};$$

$$h = (K_{max} - K_{min}) \times K_{int}^{-1} \times 100;$$

$$q = L \times F^{-1}.$$

q represents a measure of the relative magnitude of lineation and foliation, ranging in value from zero to 2.0.

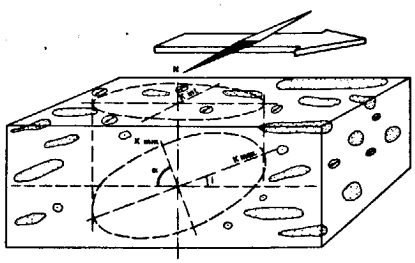

Figure 2

Orientation of the ellipsoid of magnetic susceptibility, with respect to the bedding and current direction.

Orientation de l'ellipsoïde des indices de susceptibilité magnétique en fonction du litage et de la direction des courants de fond.

ANALYTICAL PROCEDURES

Magnetic properties

The surface of a Reineck box corer is sampled using 8 cm^3 cubic containers. The remanence was measured after partial magnetic cleaning in an alternating field of 150-200 Oe. The susceptibility values are measured for 15 directions using an AC bridge. Each measurement is corrected for thermal drift and the diamagnetism of the plastic container. The 6 values of the anisotropy tensor are evaluated from the 15 measurements using a least squares method. The calculation of the matrix eigen-vector and associated eigen-values allow us to determine the orientation of the anisotropy of magnetic susceptibility ellipsoid axis (K_{max}, K_{int}, K_{min}). Knowing the orientation of the cube relatively to the north remanent magnetism, one is able to calculate the absolute orientation of the ellipsoid axis. The sedimentation rates ranging from millimeters to a few centimeters per 1 000 years, as well as mixing of the surface sediments by biological activity make clear that the secular variations of the terrestrial magnetic field are averaged out. The orientations of K_{max} are plotted on half-stereographic diagrams because they correspond to azimuths and not to directions.

Textural properties

After the magnetic measurements have been completed, the size fraction coarser than 63 μm is removed by wet sieving. Then, 9 cm^3 of the suspension (S_1) containing the silt and clay sized particles are sampled and then diluted in 250 cm^3 ordinary water (S_2), 50 cm^3 of this suspension are diluted in 150 cm^3 of an electrolyte solution for analysis with an electronic counter. Three subsamples are taken from the original suspension (S_1) and submitted to analysis. Thus the calculated particle size distribution for particles less than 63 μm is the average of three measurements.

Three more 9 cm^3 subsamples are taken from suspension S_1, from which we eliminate calcium carbonate particles, through action of HCl (30%). The excess HCl is eliminated by washing and centrifuging the residue, then the above procedure is applied.

Knowing the carbonate content of the less than 63 μm fraction, one is able to derive from the bulk and residual size distributions, those of the calcitic components less than 63 μm and then for the 63-8 μm fractions, from which we derive the median. The range of the analytical error has been evaluated. The whole analytical procedure starting with the sampling from suspension S_1, has been repeated thirty times on a sample of average lithological composition. The results show that we evaluate the median with an error of ±2 μm at the 95% confidence interval.

PRESENT-DAY CIRCULATION

Introduction

In order to test the possibility of using surface sediments as a long-period natural current meter, we have studied surface sediments in five areas, where the bottom current regime is relatively well known (Fig. 3):
1) Cape Basin; 2) Vema Channel; 3) Vema Fracture Zone; 4) Alboran Sea, and 5) Bay of Biscay continental margin. We will review the results for each of these areas in terms of the proposed model.

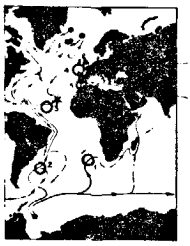

Figure 3

Studied areas: 1) *Cape Basin;* 2) *Vema Channel;* 3) *Vema Fracture Zone,* 4) *Bay of Biscay,* 5) *Alboran Sea;* 6) ★ *KR* 17; *with indication of the pattern of bottom current circulation, after Stow and Lovell* (1979).

Zones étudiées : 1) Bassin du Cap; 2) Chenal Vema; 3) Zone de Fracture Vema; 4) Golfe de Gascogne; 5) Mer d'Alboran, ★ KR 17; avec indication de la circulation profonde d'après Stow et Lovell (1979).

Regional studies

Cape Basin (Fig. 4)

During the Walvis cruise of the RV Jean Charcot, a detailed survey of a small area of the Cape Basin was

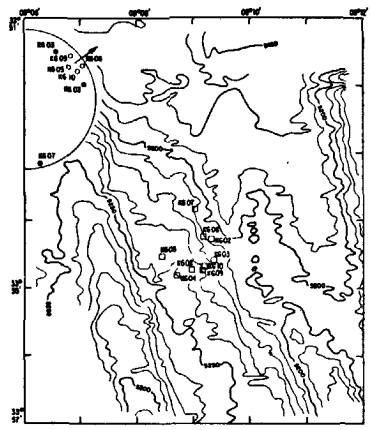

Figure 4

Bathymetric map of studied area in the Cape Basin and stereographic diagram. ●, *upper hemisphere;* ○, *lower hemisphere.*

Carte bathymétrique de la zone étudiée du Bassin du Cap avec projection stéréographique de K_{max}: ● hémisphère supérieur, ○ : hémisphère inférieur.

conducted. The survey included both bathymetry (Seabeam) and surface sediments sampling (Usnel and Reineck corers). The sea floor lies at an average depth of 5 240 m, its morphology is characterized by elongate troughs and ridges trending N 340°. Surface sediments consist of a 30 to 45 cm thick layer of siliceous pelagic clay, superimposed locally on nannofossil marly ooze of upper Pleistocene age (C. Müller, pers. comm.). The regional bottom current regime is characterized by a northeastward flux of Antarctic Bottom Water (Wüst, 1957). Lithological and magnetic data are summarized in Table 3.

The sand content of the sediment is very low (about 2%), consisting mostly of agregates. The medians of the bulk sediment range from 12 to 21 μm with an average of 15 μm, while the silt fraction medians range from 21 to 26 μm with an average of 23 μm, i.e. "average silt size" as defined in this paper. This suggests a balance between erosion and sedimentation processes and a mean velocity on the order of 1 cm/sec. The average hydrodynamic

Table 3

Lithologic and magnetic fabric parameters of Cape Basin sediments.
Lithologie et fabrique magnétique des sédiments du bassin du Cap.

	% $CaCO_3$	% sand	M_d	M_{d_s}	C_1	H(%)	Q	$\hat{\alpha}$
KG02 surf.	3	1	21	26	128	0.36	1.48	23
KG02 surf.	3	5	17	25	118	0.49	0.84	17
KG03	3	5	14	22	91	1.52	0.98	61
KG03	2,5	2	15	23	100	0.73	0.07	65
KG05 surf.	2,5	3	12,5	21,5	87	0.40	0.56	64
KG05 surf.	2,5	5	17	25	118	0.35	1.22	4
KG05 (11-13 cm)	2,5	14	19	23,5	104	0.63	1.05	42
KG06	3	3	15	24	109	0.60	0.311	81
KG06	2,5	2	13	21,5	87	0.90	1.35	37
KG07	3	5	15	23	100	0.46	1.01	69
KG09	2,5	1	12	21,5	87	0.11	1.07	7
KG09	4	1	16,5	23,5	104	0.48	0.25	59
KG10	2,5	2	12	21	83	0.36	1.76	72

$\overline{C_1} = 101$, $\overline{H} = 0.57$.

indice $\overline{C}_1$ is 100. The anisotropy of magnetic susceptibility (AMS) study provides results for 7 out of the 13 samples on the basis of $\hat{\alpha} > 50°$. An hand approximation of the average azimuth is N 55°. It suggests that the bottom current may cross at an angle the elongated ridges particularly where their axis is depressed as shown by the bathymetric map. The northern sample KR 07 indicate an azimuth (167°) roughly parallel to the bathymetric trends, thus suggesting a possible channelling of the bottom current. Anisotropy percentages range from 0.11 to 1.52% with an average of 0.56%.

Vema Channel (Fig. 5)

The Vema Channel is the only deep passage through the Rio Grande Rise, between the Argentina and Brazil Basins. It is a narrow gap, approximately 500 km

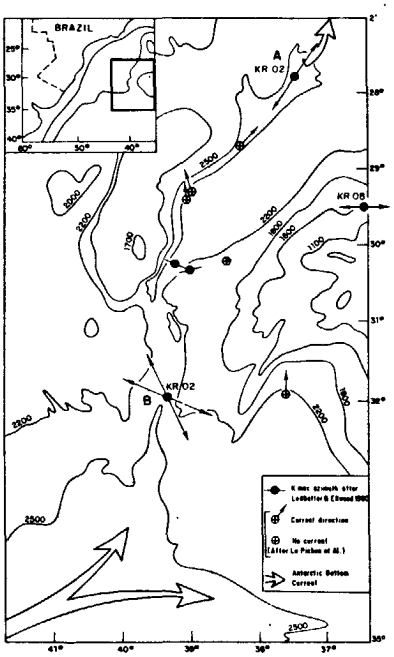

Figure 5

Bathymetric map of the Vema Channel area, and indication of bottom current azimuth from AMS measurements.

Carte bathymétrique du chenal de Vema, avec indication de l'azimuth des courants de fond d'après les mesures d'anisotropie de susceptibilité magnétique.

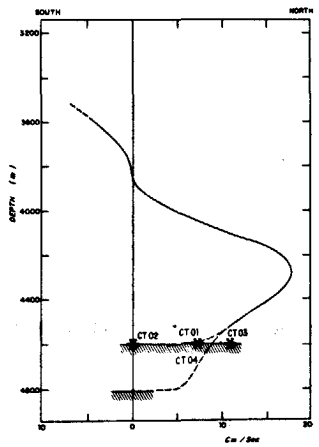

Figure 6

Computed velocity profile in the main branch of the Vema Channel after Johnson et al. (1976) *and average of current measurements at stations A and B.*

Profil des vitesses dans la branche principale du chenal Vema d'après Johnson *et al.* (1976) et moyenne des vitesses mesurées aux stations A et B.

long, and 50 km wide, with a depth of about 4 500 to 5 200 m. Antarctic Bottom Water which emanates from the Weddell Sea flows through the gap into the Brazilian Basin. This area was investigated during the Geobresil cruise of the RV Jean Charcot. Two stations at the northern (A) and southern (B) extremities of the Channel were studied in detail. Figure 6 after Johnson *et al.* (1976) illustrates the velocity profile in the main branch of the channel. The velocities were recorded at stations A and B during four short periods and the average velocity plotted on Johnson's curve (0-6 cm/sec. and 6-10 cm/sec. respectively). The lithological and magnetic properties of the sediments are summarized in Table 4. Sediments from stations A and B are clayed silty mud, the sand contents at station B exceed 10%. Nannofossil ooze covers the northern flank of the Rio Grande Rise (KR 08). South of the Vema Channel the current azimuth deduced from the direction of K_{max} of the surface sediment is N 334° and is consistent with the expected current direction (Sichler, Auffret, 1979). However, at a lower level (9-11 cm) an unexpected orientation of N 295° is found. Unfortunately no age is available for these deposits.

North of the Channel the measured azimuth (N 32°) is in very good agreement with bathymetric trends. The

Table 4

Lithologic and magnetic fabric parameters of Vema Channel sediments.
Lithologie et fabrique magnétique des sédiments du chenal Vema.

		%$CaCO_3$	%sand	M_d	M_{da}	C_1		H(%)	Q	$\hat{\alpha}$
KR 02	2.5-4.5 cm	1.5	0.2	22	30	170	159	1.01	0.81	78
	5-7 cm	2.5	0.4	22	28	148		0.73	0.77	26
KR 12	4-6 cm	1.5	7	39	40	302	317	2.43	0.9	8
	9-11 cm	1.5	11	48	42	333		2.87	0.46	73
KR 08		90	27	38	36	245		1.62	0.46	70

azimuth obtained from the northern flank of the Rio Grande Rise (N 90°) is parallel to the bathymetric contours. This shows that the North Atlantic Deep Water Current flows in a direction parallel to the Rio Grande Rise.

Silt texture and related hydrodynamic coefficients agree with the respective current velocities recorded at stations A and B. The anisotropy percentages are larger at station B (2.65%) than at station A (0.85%), which reflects the hydrodynamic significance of this parameter.

Vema Fracture Zone

The Vema Fracture Zone belongs to a system of transform faults that offset the Mid-Atlantic Ridge at latitude 11°N between 41° and 45°30W. Two elongate troughs deeper than 5000 m are present at its western border while the eastern area is characterized by a relief of 4500 m (Van Andel *et al.*, 1971). This eastern area of a high relief may act as sills for flow of Antarctic Bottom Water. Figure 7 is a detailed map of a small area from the fracture zone, obtained during a bathymetric Seabeam survey (VEMA cruise of the RV Jean Charcot), Khripounoff *et al.*, 1980). During the same cruise the Centre Océanologique de Bretagne carried out a study of AABW flow in the sill region west of the fracture zone (Vangriesheim, 1980).

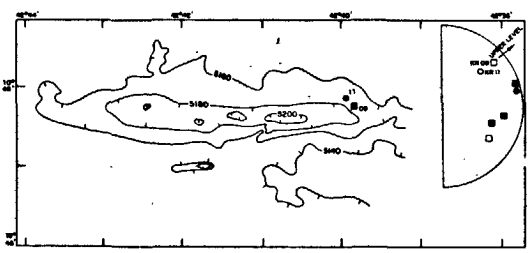

Figure 7

Bathymetric map of the studied area in the Vema Fracture Zone and polar stereographic diagram. ● ■, *uper hemisphere;* ○ □, *lower hemisphere.*

Carte bathymétrique de la région étudiée dans la Fracture Vema et projection stéréographique, ● ■ : hémisphère supérieur, ○ □ : hémisphère inférieur.

Table 5

Lithologic and magnetic fabric parameters of Vema Fracture.

Lithologie et fabrique magnétique des sédiments de la Fracture Vema.

Level		$\%CaCO_3$	% sand	M_d	M_{da}	M_{dor}	M_{dac}	C_2	C_1	H(%)	Q	$\hat{\alpha}$
KR09	5-7 cm	30	6	19	27	22	40	166	–	–	–	–
	9.5-11 cm	40	6	21	27	23	34	146	–	0.25	1.28	55
	14-16 cm	52	14	23	26	26	37	178	–	1.13	1.58	52
	17-19 cm	–	–	–	–	–	–	–	–	0.70	1.09	61
	19-21 cm	40	14	29	31	19	36	129	–	1.01	0.42	77
	21-23 cm	–	–	–	–	–	–	–	–	1.40	0.03	69
KR11	0-2 cm	–	–	–	–	–	–	–	–	0.40	1.2	21
	2-4 cm	34	9	20	26	21	35	139	–	0.82	1.2	51
	9-11 cm	34	13	27	30	21	37	147	–	1.26	1.37	50
	14-16 cm	12	3	19	26	25	31	147	–	–	–	–
	19-21 cm	39	12	25	26	23	33	134	–	1.05	0.35	59
	23-25 cm	3	8	31	28	–	–	–	–	0.38	0.11	10
KR17	5-7 cm	2	0	24	26	–	–	–	127	0.43	1.22	29
	18-20 cm	8	0.3	23	25	26	31	152	–	1.25	0.38	79
	23-25 cm	9	0.3	19	26	30	39	51	–	0.45	1.19	3

Two close Reineck cores were taken west of the sill and one to the east in the Gambia Basin (KR 17). The lithologic and magnetic data are summarized in Table 5. Core K 9 consists of marly nannofossil ooze ranging from 30 to 52% $CaCO_3$, and 6 to 14% sand. Core KR 11 is very similar to KR 9, but contains interbedded mud levels. Core KR 17 is comprised of mud, with a very low carbonate and sand content. Van Andel *et al.*, (1971) indicate that high rates of sedimentation prevail in the Vema Fracture Zone hence the upper 30 cm of the sediment could be of Holocene age. The azimuth of the ellipsoid longest axis, has been evaluated using data from cores KR 9 and KR 11. The plot of the azimuth on the stereographic diagram shows a wide dispersion. However, the topmost sample from each core indicate a N 50° azimuth while the lowermost samples are relatively scattered around N 90°.

There is no positive correlation between the median of the residual and calcitic silt fractions.

The dispersion of the azimuths and the lack of textural correlation may be related to lateral input of sediment from gravity controlled current generated on the fracture walls and/or to the rather complex current regime resulting from the "overflow" of the eastern sills.

The average anisotropy percentages in cores KR 9 and KR 11 is relatively low (0.84) and highly variable ($\sigma \doteq 0.4$), which again may be related to the variability of the flow regime.

Alboran Sea

The Alboran Sea (Fig. 8) constitutes the westernmost part of the West Mediterranean Basin and consists of two small basins connected by a narrow strait: the Alboran Trough. The average inflow of Atlantic Surface Water into the Mediterranean (10^6 .sec.$^{-1}$) implies a mean velocity of 2 cm.sec.$^{-1}$ for the outflowing undercurrent for a cross-section of $5 \times 10^7 m^2$. Near bottom measurements achieved during the Polymède cruise of the RV Jean Charcot indicate that locally current velocities may range from 5 to 10 cm.sec.$^{-1}$ (Auffret, unpublished data).

According to Frazer *et al.* (1970) the Western Alboran Basin and the southern part of the Eastern Basin are covered by calcareous mud, whereas marly ooze occupies the north and east of the Eastern Basin.

Figure 8

Bathymetric map of the Alboran Sea and indication of the bottom current azimuth provided by AMS measurements.

Carte bathymétrique de la mer d'Alboran, avec indication de l'azimuth des courants de fond déduit de l'anisotropie de susceptibilité magnétique.

The lithologic and magnetic properties of the studied sediments are summarized in Table 6. Only two samples fulfilled the acceptable magnetic criteria. Both samples gave a flow azimuth of N 70°, consistent with the physiographic setting (Sichler, Auffret, 1979). The average value of C_2 coefficient is 180. The calculated C_3 value (+136) indicates a positive correlation between the median of the calcitic and residual fractions and points to current control deposition, as previously shown (Auffret *et al.*, 1974). The percentage of anisotropy ranges between 1.14 and 1.92 and averages 1.5. This relatively high value is consistent with the hydrodynamic index.

Bay of Biscay continental margin

The area of study is known as the Meriadzek Terrace (Fig. 9). North Atlantic Bottom Water is in contact with the sea floor at a depth between 2 000 and 3 200 m. This water mass is effected by rotating bottom currents of semi-diurnal tidal periodicity, the velocities of which

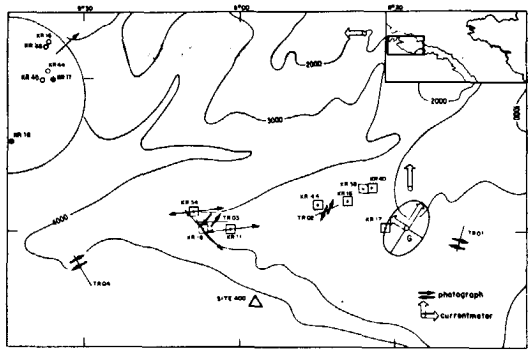

Figure 9

Bathymetric map of the Celtic margin, localisation of cores and stereographic diagram of samples from the eastern area. ●, upper hemisphere. ○, lower hemisphere.

Carte bathymetrique de la marge celtique, localisation des prélèvements et projection stéréographique de l'indice K_{max} des échantillons de la zone est ● : hémisphère supérieur, ○ : hémisphère inférieur.

Table 6

Lithologic and magnetic fabric parameters of Alboran Sea sediments.

Lithologie et fabrique magnétique des sédiments de la mer d'Alboran.

Level		% $CaCO_3$	% sand	M_d	M_{ds}	M_{dsr}	M_{dsc}	C_2	H(%)	Q(%)	$\hat{\alpha}$
KR 33	0.5-2.5 cm	23	7	17	26	20	44	166	1 74	0 40	9
	7.5-9.5 cm	25	4	15	26	17	59	190	1.22	1.89	69
KR 34	6-8 cm	20	4	13	26	19	46	165	1 68	0.45	5
	13-15 cm	21	4	12	20	19	30	108	1.14	1 03	54
KR 36	3-5 cm	19	3	22	29	21	50	198	1.24	0.30	3
KR 39	29-31 cm	19	3	26	32	22.5	57	242	1.92	0.94	11
KR 41		25		21.5	30	22	46	191	1.50	0.51	2

Table 7

Lithologic and magnetic fabric parameters of Meriadzek Terrace sediments.

Lithologie et fabrique magnétique des sédiments de Meriadzek.

	% $CaCO_3$	% sand	M_d	M_{ds}	M_{dsr}	M_{dsc}	C_2	H(%)	Q	$\hat{\alpha}$
KR 11 (6-8 cm)	62	42	51	29	20	35	132	3.33	0.67	17
KR 16 (1-3 cm)	54	41	51	31	22	38	158	2.11	0.77	10
KR 16 (5-7 cm)	55	38	47	33	23	47	204	2.32	0 55	2
KR 16 (18-20 cm)	39	32	40	32	24	46	209	3.49	0.73	28
KR 16 (21-23 cm)	35	32	42	29	22	50	208	2.99	1.08	71
KR 17 (2-4 cm)	55	14	23	27	18	38	129	2.28	0.35	5
KR 17 (4-6 cm)	54	13	23	27	18	36	126	3.02	1.25	26
KR 17 (21-23 cm)	54	14	22	26	20	38	144	2.65	0.25	19
KR 18 (6-8 cm)	59	42	61	30	20	34	129	2.58	0.63	70
KR 34 (4-6 cm)	55	44	56	30	21	43	171	2.04	0.97	26
KR 38 (0-2 cm)	57	25	28	27	22	39	162	2.06	0.88	22
KR 38 (4-6 cm)	56	22	25	25	18	34	116	2.01	1.54	1
KR 38 (19-21 cm)	51	19	24	25	24	28	127	2.48	0.50	30
KR 40 (2-4 cm)	55	17	32	33	19	44	158	1.22	0.73	9
KR 40 (21-23 cm)	50	9	21	24	22	29	118	3.32	0.74	50
KR 44 (2-4 cm)	56	20	25	25	19	36	129	1.92	0.28	1
KR 44 (16-18 cm)	54	16	23	25	19	30	108	1.08	1.46	19

reach a maximum of 25 cm.sec.$^{-1}$ (Gould, MacKee, 1973; Auffret *et al.*, 1975). Bottom current action on the sediments is evidenced by lineations and ripple-marks observed on sea-floor photographs. The surficial sediments of the eastern part consist of nannofossil foraminifer ooze, the sand fractions of which average 21 %. Toward the west the carbonate contents decrease slightly, while sand contents increase and range from 35 to 91 %. Lithologic and magnetic data have been summarized in Table 7. Only three samples were acceptable on magnetic criteria due to lower than normal $\hat{\alpha}$ values ($\alpha < 50°$) (Coleno, 1980). However, the orientations of K_{max} appear very consistent especially for samples from the eastern area, here most flow azimuths are aligned north-northeast, which is also the predominant direction of the bottom currents.

The correlation coefficient between the median of silt carbonate and non-carbonate fraction calculated on 14 samples (from the first 20 cm of the cores), reaches a value of +0.65, while the hydrodynamic indice C_3 is +93, and C_2 averages 148. The anisotropy percentages of these 14 samples range between 1.08 and 3.49, and average 2.29. This high value is consistent with the indication of the hydrodynamic index.

Figure 10

Relation between 1) hydrodynamic index (C_1 and C_2) and mean current velocities (✱); 2) average anisotropy percentages and mean current velocities (✱). The dashed and full lines are best fit hand approximations.

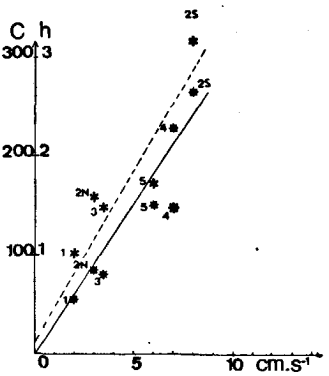

Relation entre : 1) le coefficient d'hydrodynamisme (C_1 et C_2) et la vitesse moyenne des courants de fond (✱); 2) le pourcentage moyen d'anisotropie et la vitesse moyenne (✱). Les droites ont été tracées d'après une approximation visuelle.

Discussion

Current intensity

The mean velocity for each station has been evaluated using sources of various origins and of very different quality; their evaluation and the related references are summarized in Table 8. There exists a possible positive correlation between the average of the hydrodynamic indices C_1 and C_2 and the mean current velocity (fig. 10). The relationship between the Alboran Sea and Meriadzek Terrace values of mean velocities with respect to the mean hydrodynamic index and average current velocity is depicted in Figure 10. The relationship shown here is the reverse of that which one might expect. Possible explanations include an influx of coarse carbonate sedimentation, or a bad estimation of the respective mean current velocity. In both areas, however, a positive correlation has been found between median size of the carbonate and non-carbonate silt fractions, pointing to a current-controlled sedimentation regime.

Such a correlation has not been demonstrated in surface sediment of the Vema Fracture Zone. The average anisotropy percentage of the different stations also appear positively correlated with the average velocity (Fig. 10), thus confirming the hydrodynamic significance of this parameter. Obviously, these relations need confirmation through long term current monitoring and appropriate sampling.

Current directions

The azimuths of flow directions provided by the orientation of the longest axis of the ellipsoid of magnetic susceptibility is most often in agreement with the expected orientation (i.e. parallel). Ellwood and Ledbetter (1979) have interpreted data from the eastern flank of the Vema Channel as indicative of an orientation of the ellipsoid long axis normal rather than parallel to the current direction. According to these authors, these may be expected for high-velocity bottom currents. According to Johnson's data (Fig. 6) the level of their samples (4 100 to 4 200 m) corresponds to current velocity averaging 10 cm/sec. as in station B, where the direction was found parallel to the prevailing direction.

We agree with Ledbetter and Ellwood (1980) in that elongated particles when transported should roll on the bottom but once deposited they should probably reorient themselves parallel to flow lines.

Table 8

Evaluation of average current velocities.

Évaluation des vitesses moyennes des courants de fond.

Area		Mean speed	Max speed	Height above bottom (m)	Method: Hydrographic	Method: *in situ*	Time	C	h(%)	References
Cape Basin		2 cm/sec.	–	–	+	–	–	101	0.56	Wüst (1957)
South Vema Channel	CT 3	10 cm/sec.		1.5	–	+	30 min.	317	2.65	Auffret *et al.* (1975 *a*)
	CT 4	6 cm/sec.		1.5	–		44 min.			Auffret *et al.* (1975 *a*)
North Vema Channel	CT 01	6 cm/sec.		1.5		+	44 min.	159	0.85	*Idem*
	CT 02	<1 cm/sec.		1.5		+	80 min.			*Idem*
Vema fracture zone	ST 4	4 cm/sec.	12 cm/sec.	10	–	+	26 days	148	0.8	Vangriesheim (1980)
	ST 5	3 cm/sec.	12 cm/sec.	10	–	+	8.5 days			
Alboran basin	ST 54	6 cm/sec.	10 cm/sec.	1	–	+	7 hrs.	172	1.5	Auffret, unpublished data
Meriadzek terrace	CT 02	7 cm/sec.	20 cm/sec.	1	–	+	9 hrs.	148	2.29	Auffret *et al.* (1975 *b*).

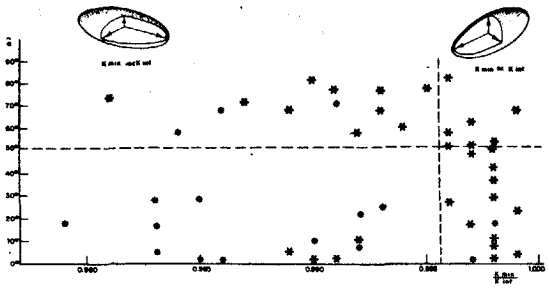

Figure 11

Relation between $K_{max} \times K_{int}^{-1}$ *and* $\hat{a}$ *values.* ● *samples from the Meriadzek Terrace.*

Relation entre $K_{max} \times K_{int}^{-1}$ et les valeurs de $\hat{a}$, ● échantillons de Meriadzek.

Studies of natural sediments, in conjunction with laboratory experiments (Rees, 1965) suggest that fabrics produced during grain-by-grain deposition commonly correspond with q values ranging from 0.06 to 0.67. This observation has been used by some authors to assess the validity of their data.

For abyssal plain environments, a subvertical minimum axis ($\alpha > 50°$) of the ellipsoid appears to be a sufficient sample criteria. All sediment surface samples fulfilling this requirement have supplied bottom current azimuth consistent with expected directions. However, the magnetic fabric of margin surface sediments appears quite different. A few samples with α values lower than 50°, also have relatively significant anisotropy percentages. The consistency of the current azimuth data provided by the magnetic fabric, particularly in zone 1 of the Meriadzek Terrace, suggests the need to consider possible sources of disturbance of the ellipsoid orientation.

It appears from Figure 11 that angle α is characterized by a larger dispersion for values of $K_{min} \times K_{int}^{-1}$ larger than 0.995. However, this relationship does not hold for margin samples, which are also generally characterized by lower angle α values. The reason for this is not immediately obvious, but three possible factors include:

1) the influence of bioturbation which would destroy the foliation but preserve the lineation in sediments comprising strongly elongated magnetic particles (high shape anisotropy);

2) a particular fabric resulting from the oscillatory motion induced by semi-diurnal tidal currents;

3) soft sediment deformation, related to creeping of the surface sedimentary layer on a very gentle slope.

According to von Rad (1970) the imbrication angle could be considered as an indicator for the flow direction. In this study we have not yet reached any conclusion for or against this assessment. Obviously factors such as grain sizes, slope of the sea-floor, oscillating current regime may interfer. A final conclusion should be possible only after experimental work and *in situ* investigations on a statistical basis.

PALEOCIRCULATION STUDIES

Introduction

Paleoenvironmental studies rely upon many sources of information, including mineralogy of detrital or authigenic mineral, micropaleontology, and geochemistry. Among those factors that are relevant for the reconstruction of the paleoenvironment, bottom currents are one of the most important. Carbonate accumulation rates, for example, appear to be under the control of productivity and dissolution, that in turn are partly dependent on the turn-over rates of water masses and the intensity of bottom currents (Berger, 1970; 1974; Schink, Guinasso, 1977). Sedimentary hiatuses also, are often explained as the consequence of a strengthening of bottom current velocity (Fischer, Arthur, 1977; Auffret, Pastouret, 1978; 1979). But appreciation of the importance of the deep circulation has remained until now rather subjective. However, Diester-Haas (1973; 1975) has already shown that textural parameters of the carbonate fraction of sand-sized particles could be used in order to demonstrate fluctuation of the paleocirculation. Ellwood and Ledbetter (1977) also have used the textural parameters of silt fractions, in order to evaluate paleocirculation fluctuations. We use here a new hydrodynamic index:

$$C_4 = \overline{M}_{dsr} \times \overline{M}_{dsc} \times (23^2)^{-1} \times r \times 100,$$

in which $\overline{M}_{dsr}$ and $\overline{M}_{dsc}$ are the averages of silt medians of core samples from a given stratigraphic interval.

We present below the results of textural studies in two sedimentary sections drilled by the Glomar Challenger. The first one consists of Eocene and Oligocene sediments from DSDP Leg 48 Site 400 in the Bay of Biscay (Montadert *et al.*, 1979), the second one of lower and middle Miocene sediments from DSDP Leg 42, Site 372; in the Western Mediterranean (Hsü *et al.*, 1978).

One point which we have disregarded in the case of surface sediment cannot be overlooked in the case of older sediments. Diagenetic reaction effects are bound to become more common with increasing overburden on the sediments. Precipitation of $CaCO_3$ may lead to overgrowths on carbonate shell debris, or authigenic carbonates. The occurrence of such processes is often related to deep burial (more than 1 000 m sediment), however evidence of such processes is often obvious, from lithological examination and geochemical analysis such as the evaluation of $^{18}O/^{16}O$ ratio from planktonic shells debris. Sections affected by recrystallisation should of course be rejected, as non pertinent for our purpose.

Site 400, Eocene, Oligocene section

We have sampled from site 400 A, drilled at the foot of the Celtic margin (47°22, 90°N, 9°11, 90'W), an Eocene-Oligocene section 140 m thick (Auffret, Pastouret, 1979).

During early and middle Eocene, marly nannofossil chalk and siliceous mud have been accumulating at the rate of 1.3 cm/1 000 years. Sponge spicules and

Table 9
Hydrodynamic index of sediments from hole 400 *(leg* 48*) and hole* 372 *(leg* 42*).*

Coefficient d'activité hydrodynamique des sédiments des forages 400 (leg 48) et 372 (leg 42).

Period	Samples	$M_{dr}(\mu)$	$M_{dc}(\mu)$	r	C_4
Site 400 :					
Early Eocene	5	23	19	−0.82	−67
Middle Eocene	6	19	20	0.83	60
Oligocene	11	22	35	0.64	93
Lower Miocene	5	20	15	0.93	53
Site 372 :					
Late Burdigalian-Langhian	13	16	26	0.94	73
Serravallian	9	13	26	0.16	10

manganese debris (interpreted by Debrabant and Foulon (1979) as indicative of oceanic currents) become important constituents of the sediment coarse fraction near the top of the middle Eocene section, which is also characterized by the occurrence of silty laminae. The upper Eocene corresponds to a sedimentary hiatus, while the Oligocene consists of a 45 m thick section of chalk and marly nannofossil chalk, which has been deposited at the rate of 0.35 cm/1 000 years. It also exhibits numerous coarse cross-bedded intervals which consist mostly of sponge spicules.

The analytical results have been summarized in Table 9 and are illustrated in Figures 12 and 13. The correlation coefficient for lower Eocene sediments is negative, which we interpret as indicative of an hemipelagic sedimentation and low current regime. The correlation coefficient for the middle Eocene section (0.83) is high and significant (6 samples); it points to a strengthening of the hydrodynamic control, which is corroborated by the sedimentary structures and the coarse fraction composition. This enhancement of the hydrodynamic control just precedes the upper Eocene hiatus. The Oligocene correlation coefficient (0.64) is significant (11 samples) and the hydrodynamic index reaches a value of 93. This high value is corroborated by a reduction of the

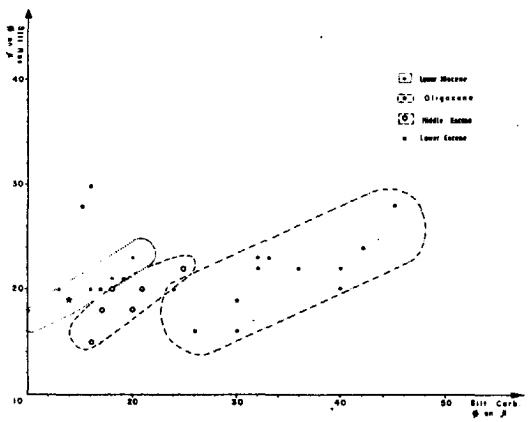

Figure 12
Relation between median of calcitic and residual silt in hole 400*. Eocene to Lower Miocene sediments.*

Relation entre les médianes des silts carbonatés et résiduels dans les sédiments miocène inférieur à éocène du forage 400.

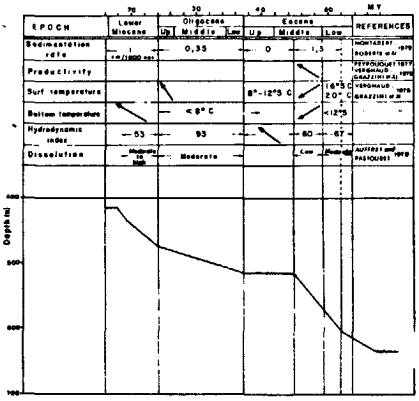

Figure 13
Evolution of hydrodynamic index at site 400 *in relation with other paleoenvironmental indicators.*

Évolution comparée du coefficient d'hydrodynamisme et des autres indicateurs du paléoenvironnement au site 400.

sedimentation rates and the occurrence of sandy contourites (spiculite), which suggest the existence of an extensive sponge field, on a well-ventilated bottom. A major hydrologic change is thought to have occurred between early and middle Eocene in the Bay of Biscay. Increasing productivity is suggested by high opaline silica accumulation rates, high phosphorus content suggested by the ostracod assemblage (Ducasse, Peypouquet, 1979), and low ^{13}C contents (Vergnaud-Grazzini *et al.*, 1978). According to the last authors, the $^{18}O/^{16}O$ isotopic ratio of carbonate from hole 398 (Leg 47 B) (Sibuet *et al.*, 1979) points to a marked cooling of surface and bottom waters at that time. Thus our results are in good agreement with the conclusions obtained independently by different authors, all of them leading to evidence of an enhancement of the bottom circulation regime at the early-middle Eocene transition. This active circulation regime also prevailed during the late Eocene and the Oligocene, where the bottom water temperatures decreased to less than 8°C.

Site 372, Miocene (Fig. 14)

Hole 372 A was drilled during Leg 42 on the Minorca rise in the Western Mediterranean basin (40°01.90′N; 4°47.79′E).

Unit 4 is composed of mudstone and nannofossil marlstone. Intercalation of graded and laminated sandstone and siltstone at the base of the unit and suspected high sedimentation rates (31.2 cm/1 000 years) lead us to reject this section for paleocirculation estimate by our method.

Unit 3 B (core 33-21) is composed of upper Burdigalian and Langhian nannofossil chalk, that have accumulated at the rate of 10.5 cm/1 000 years. It corresponds approximately to the NN 4 nannofossil zone. The sediments are intensely bioturbated. The correlation coefficient (0.94; 13 samples) and the hydrodynamic index (73) for this interval are high, thus reflecting the influence of bottom water circulation, which is

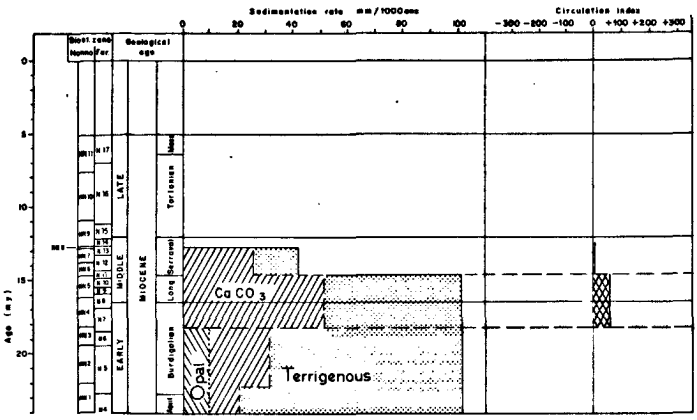

Figure 14

Evolution of hydrodynamic index at site 372 in relation with other paleoenvironmental indicators.

Evolution comparée du coefficient d'hydrodynamisme au site 372 et des autres indicateurs du paléoenvironnement.

corroborated by ostracods assemblages that point to high dissolved oxygen contents (Benson, 1978).

Unit 3 A (cores 21 to 972) is composed of Serravallian chalk that are devoid of bioturbation structures. The accumulation rate is lower than in the underlying unit (4.2 cm/1 000 years). The low correlation coefficient (0.16-9 samples) and hydrodynamic index (10) are corroborated by ostracod assemblages that indicated a lowering of the dissolved oxygen contents, i.e.: little bottom water circulation.

Thus we observed at the Langhian-Serravallian transition a marked decrease of the bottom water circulation, simultaneously with a reduction of terrigenous and carbonate components sedimentation rates, reduction of dissolved oxygen and traces of benthic activity, and important fluctuations in $^{18}O/^{16}O$ ratio of planktonic and benthic foraminifers (Vergnaud-Grazzini, 1978). All these facts point to a slowing of the bottom water circulation that may either indicate an interruption of bottom water formation inside the basin, or the closure of a deep and narrow sea-way between the West-Mediterranean Basin and the Atlantic Ocean.

CONCLUSION

In this paper we have presented the theoretical framework and a model to predict hydrodynamic conditions at the bottom boundary layer from textural and magnetic fabric studies. Studies of recent deep-sea surface sediments show that the texture of the silt fraction is correlated to bottom current intensities. Moreover, where action of the bottom currents is predominant, there is a positive correlation between median size of the carbonate and non-carbonate silt fraction. The magnetic fabric of the sediment, as characterized by the orientation of the ellipsoid of magnetic susceptibility, appears to us as an extremely sensitive indicator of the current azimuth. In abyssal plain environments, the criterion of subverticality of the minimum axis appears to be a sufficient requirement; this allows us to obtain orientations that are consistent with expected current directions. In margin environments, the criterion of subverticality of the minimum axis seems very restrictive; further studies are needed on this point.

In general, a relationship between hydrodynamic indices, the percentage of anisotropy of the magnetic susceptibility and estimated average velocity of the bottom current can be demonstrated.

As a matter of fact, many sedimentologists concerned with deep-sea deposits have recently recognized often independently that "*...there should be differences in the particle size distributions of fine deposits formed by slow particles settling as compared to those that have been influenced by bottom currents...*" (Gorsline, 1980). Indeed this becomes more and more commonly demonstrated for surficial deposits, the only limitation being the availability of particles in the silt-size range. The control of the hydrodynamic significance of the textural properties on two different particles groups as proposed eralier by Barusseau (1973) and Diester-Haass (1973; 1975) appears to us of primary importance.

As far as carbonates made up one of these fractions, the question of the relationships between rate of dissolution and bottom current intensities arises immediately; this should be clarified by further investigations. The application of the method to past deposits has two prerequisites to fulfill:

1) the studied section should have been deposited under the control of "normal" oceanic current;

2) diagenetic effect (late dissolution, precipitation, overgrowth...) should not have occurred.

These two conditions must be clearly established before any attempt to the reconstruction of a paleo bottom current regime. A general assessment about future work in this field is that they will have to be grounded on a well defined statistical basis.

Acknowledgements

Our work is based on samples collected on board RV Jean Charcot during several cruises: Geobrésil, Vema, Walvis, Polymède, Biogas. We are greatly indebted to the officers, crew, scientists and technicians who have participated. Suzanne Marques and René Kerbrat have

been in charge of the sedimentological analysis. We thank also July Fisher, Daniel Carré and Nicole Guillo-Uchard, and the referees for helping us to produce this work.

REFERENCES

Arrhenius G., 1963. Pelagic sediments, in: *The Sea*, **3**, edited by M. N. Hill, New York, Wiley Interscience, 655-727.

Auffret G. A., Pastouret L., 1975. Processus sédimentaires actuels dans le Vema Channel (Atlantique Sud), *IX^e Congrès International de Sédimentologie, Nice*, Thème 8, 1-5

Auffret G. A., Pastouret L., 1978. La fraction silteuse des sédiments, traceur de l'intensité des courants profonds; application à la sédimentation tertiaire dans le Golfe de Gascogne, *Réun. Ann. Sci. Terre, Orsay.*

Auffret G. A., Pastouret L., 1979. Upper Cretaceous to Quaternary sedimentary processes in the Bay of Biscay from textural, mineralogical and coarse fraction studies, in: *Initial Reports of the Deep-Sea Drilling Project*, **48**, edited by L. Montadert, D. G. Roberts *et al.*, Washington, US Gov. Print. Off., 791-829.

Auffret G. A., Pastouret L., Kerbrat R., 1975. Dynamique sédimentaire au bas de la marge continentale armoricaine; exemple de la ride Aegis, Actes IX, *IX^e Congrès International de Sédimentologie, Nice*, thème 6, 1-5.

Auffret G. A., Pastouret L., Chamley H., Lanoix F., 1974. Influence of the prevailing current regime on sedimentation in the Alboran Sea, *Deep-Sea Res.*, **21**, 839-849.

Barusseau J. P., 1973. Évolution du plateau continental rochelais (Golfe de Gascogne) au cours de l'Holocène. Les processus actuels de la sédimentation, *Thèse Doct. État, Sci. Nat.*, 363 p.

Barusseau J. P., Vanney J. R., 1978. Contribution à l'étude du modèle des fonds abyssaux. Le rôle géodynamique des courants profonds, *Rév. Géogr. Phys. Géol. Dyn.*, **2**, 15, 1, 59-94.

Benson R. H., 1978. The paleoecology of the ostracodes of DSDP Leg 42 A, in: *Initial Reports of the Deep-Sea Drilling Project*, **42**, edited by K. J. Hsü, L. Montadert *et al.*, Part 1, Washington, US Gov. Print. Off., 777-783.

Berger W. H., 1970. Biogenous deep-sea sediments fractionation by deep-sea circulation, *Geol. Soc. Am. Bull.*, **81**, 1385-1402.

Berger W. H., 1974. Deep-sea sedimentation, in: *The geology of the continental margin*, edited by C. A. Burck and C. L. Drake, Springer-Verlag, Berlin, Heidelberg, New York, 213-241.

Coleno B., 1980. Anisotropie de susceptibilité magnétique dans les sédiments et courants profonds. Test de la méthode, *Mém. DEA, Univ. Bretagne Occidentale*, Brest, 52 p. (non publié).

Craig J. D., 1979. Geological investigation of equatorial North Pacific sea-floor: a discussion of sediment redistribution, in: *Marine geology and oceanography of the Pacific manganese nodule province*, Plenum Publishing Corporation.

Debrabant P., Foulon J., 1979. Expression géochimique des variations du paléoenvironnement depuis le Jurassique supérieur sur les marges nord-atlantiques, *Oceanol. Acta*, **2**, 4, 469-475.

Diester-Haass L., 1973. No current reversal at 10 000 BP, in the Straits of Gibraltar, *Mar. Geol.*, **15**, M 1-9.

Diester-Haass L., 1975. Influence of deep-oceanic currents on calcareous sands off Brazil, *IX^e Congrès International de Sédimentologie, Nice*, thème 8, 25-28.

Ducasse O., Peypouquet J. P., 1979. Cenozoic Ostracoda. Their importance for bathymetry, hydrology and biogeography, in: *Initial Reports of Deep-Sea Drilling Project*, **48**, edited by L. Montadert, D. G. Roberts *et al.*, Washington, US Gov. Print. Off., 343-352.

Eittreim S., Ewing M., 1972. Suspended particulate matter in the deep waters of the North American Basin, in: *Studies in physical oceanography*, **2**, edited by A. L. Gordon, Gordon and Breach, New York, 123-168.

Ellwood B. B., Ledbetter M. T., 1977. Antartic bottom fluctuations in the Vema Channel: effects of velocity changes particle alignment and size, *Earth Planet. Sci. Lett.*, **35**, 2, 189-198.

Fischer A. G., Arthur M. A., 1977. Secular variations in the pelagic realm, *SEPM Spec. Publ.*, **25**, 19-50.

Frazer J. Z., Arrhenius G., Hanop J. S., Hawkins D. L., 1970. *Surface sediment distribution, Mediterranean Sea*, prepared by the Scripps Institution of Oceanography for US Fleet. Numerical Weather Center 1-8.

Gennesseaux M., Guibout P., Lacombe H., 1971. Enregistrement de courants de turbidité dans la vallée sous-marine du Var (Alpes-Maritimes), *C.R. Acad. Sci. Paris*, **273**, 2456-2459.

Gonthier E., Klingebiel A., 1973. Faciès et processus sédimentaires dans le canyon sous-marin Gascogne, *Bull. Inst. Géol. Bassin Aquitaine*, **13**, 163-262.

Gorsline D. S., 1980. Deep-water sedimentologic conditions and models, *Mar. Geol.*, **38**, 1-21.

Gould W. J., Mac Kee W. D., 1973. Vertical structure of semi-diurnal tidal currents in the Bay of Biscay, *Nature*, **244**, 5411, 88-91.

Grousset F., 1977. Étude géologique du Quaternaire terminal de la zone Meriadzek-Trevelyan (Golfe de Gascogne), *Bull. Inst. Géol. Bassin Aquitaine*, **22**, 75-122.

Hamilton N., 1967. Laboratory redeposition studies; an apparaisals of apparatus and technic, in: *Method in paleomagnetism*, Elsevier, Amsterdam, London, New York, 596-603.

Hamilton N., Rees A. I., 1970. The use of magnetic fabric in paleocurrent estimation, in: *Paleogeophysics*, Academic Press, 445-464.

Heezen B. C., Hollister C. D., 1964. Deep-sea current evidence from abyssal sediments, *Mar. Geol.*, **1**, 141-174.

Hollister C. D., Heezen B. C., 1972. Geologic effects of ocean bottom currents, in: *Studies in physical oceanography. A tribute to G. Wust*, edited by A. L. Gordon, Gordon and Breach, N.Y. 37-66.

Hsü K. J., Montadert L., Garrison R. B., Fabricius F. H., Kidd R. B., Muller C., Cita M. B., Bizon G., Wright R. C., Erickson A. J., Bernoulli D., Melières F., 1978. *Initial Reports of the Deep Sea Drilling Project*, **42**, Part 1, Washington, US Gov. Print. Off.

Huang T. C., Watkins N. D., 1977. Contrasts between the Bruhnes and Matuyama sedimentary records of bottom water activity in the South-Pacific, *Mar. Geol.*, **23**, 113.

Johnson D. A., McDowell S. E., Sullivan L. G., Biscaye P. E., 1976. Abyssal hydrography, nephelometry, currents and benthic boundary layer structure in the Vema Channel, *J. Geophys. Res.*, **81**, 33, 5771-5786.

Keller G. H., Lambert D., Rowe G., Staresinio N., 1973. Bottom currents in the Hudson Canyon, *Science*, **180**, 181-183.

Khripounoff A., Desbruyères D., Chardy P., 1980. Les peuplements benthiques de la faille Vema : données quantitatives et bilan d'énergie en milieu abyssal, *Oceanol. Acta*, **3**, 2, 187-198.

Ledbetter M. T., Ellwood B. B., 1980. Spatial and temporal changes in bottom-water velocity and direction from analysis of particle size and alignment in deep-sea sediment, *Mar. Geol.*, **38**, 245-261.

Kuenen P. H., 1950. Turbidity currents of high density, *18th Int. Congr. London, Rep.*, Pt. 8, 44-52.

Kuenen P. H., 1967. Emplacement of flysch-type sand beds, *Sedimentology*, **9**, 203-243.

Kuenen P. H., Migliorini C. I., 1950. Turbidity currents as cause of graded bedding, *J. Geol.*, **58**, 91-127.

McCave I. N., Swift S. A., 1976. A physical model for the rate of deposition of fine grained sediments in the deep-sea, *Bull. Geol. Soc. Am.*, **87**, 541-546.

Middleton G. V., Hampton A. M., 1976. Subaqueous sediment transport and deposition by sediment gravity flows, in: *Marine sediment transport and environmental management*, edited by D. J. Stanley and D. J. P. Swift, John Wiley and sons, 197-218.

Montadert L., Roberts D., Auffret G. A., Bock W. D., Dupeuble P. A., Hailwood E. A., Harrisson W., Kagami H., Lumsden D. N., Muller C., Schnitker D., Thompson R. W., Thompson T. L., Timofeev P. P., 1979. *Initial Reports of the Deep-Sea Drilling Project*, **48**, US Gov. Print. Off.

Moore D. G., 1969. Reflection profiling studies of the California continental borderland: structure and quaternary turbidite basin, *Geol. Soc. Am. Spec. Pap.*, **107**, 142 p.

Mutti E., Ricci-Lucchi F., 1972. Le torbiditi dell' Appenino settentrionale : introduzione all' analisi di facies, *Mem. Soc. Geol. Ital.*, **11**, 161-199.

Nelson D. D., Pierce J. W., Colquhoum D. D., 1973. Sediment dispersal by cascading coastal water, *Geol. Soc. Am. Abstr. Progr.*, **8**, 423-424.

Nelson H., Mutti E., Ricci Lucchi F., 1977. Upper Cretaceous resedimented conglomerates at Wheeler Gorge, California: description and field guide. A discussion, *J. Sediment. Petrol.*, **47**, 926-928.

Oser R. K., 1972. Sedimentary components of northwest Pacific pelagic sediments, *J. Sediment. Petrol.*, **42**, 461-467.

Peng T. H., Broecker W. S., Kipphut G., Shackelton N., 1977. Benthic mixing in deep sea cores, as determined by C14 dating, and implication regarding climate, stratigraphy and the fate of fossil fuel CO_2, in: *The fate of fossil fuel CO_2 in the oceans*, edited by N. R. Anderson and A. Malahoff, Plenum Press, New York, London, 335-374.

Peypouquet J. P., 1977. Les Ostracodes et la connaissance des paléomilieux profonds. Applications au Cénozoïque de l'Atlantique nord-oriental, *Thèse Doct. Sci., Univ. Bordeaux-I*, 443 p.

Rees A. I., 1965. The use of anisotropy of magnetic susceptibility in the estimation of sedimentary fabric, *Sedimentology*, **4**, 257-271.

Rees A. I., 1968. The production of preferred orientation in concentrated dispersion of elongated and flattened grains, *J. Geol.*, **76**, 457-465.

Rowe G. T., 1974. The effects of the benthic fauna on the physical properties of deep-sea sediments, in: Deep-sea sediments. *Marine Sciences n°* 2, Plenum Press, New York, London. 381-400.

Rusnak G. A., 1957. The orientation of sand grains under conditions of unidirectional fluid flow. 1 Theory and experiment, *J. Geol.*, **65**, 384-405.

Schink D. R., Guinasso N. L. Jr, 1977. Modelling the influence of bioturbation and other processes on calcium carbonate dissolution at the sea-floor, in: *The fate of fossil fuel CO_2 in the oceans*, edited by N. R. Andersen and A. Malahoff, Plenum Press, New York, London, 375-399.

Shepard F. P., Mac Loughlin P. A., Marshall N. F., Sullivan G. G., 1977. Current-meter recording of low-speed turbidity currents, *Geology*, **5**, 297-301.

Sibuet J. C., Ryan W. B. F., Arthur M. A., Barnes R. O., Habib D., Iaccarino S., Johnson D., Lopatin B., Maldonado A., Moore D. G., Morgan G. E., Rehault J. P., Sigal J., Williams A. C., 1979. *Initial Reports of the Deep Sea Drilling Project*, **47**, Part 2, Washington, US Gov. Print. Off.

Sichler B., Auffret G. A., 1979. L'anisotropie de susceptibilité magnétique des sédiments : un outil pour l'étude des paléocourants, *7e Réun. Ann. Sci. Terre*, 428.

Stow D. A. V., Bowen A. J., 1978. Origin of lamination in deep sea, fine-grained sediments, *Nature*, **274**, 324-328.

Stow D. A. V., Lovell J. P. B., 1979. Contourites: their recognition in modern and ancient sediments, *Earth Sci. Rev.*, **14**, 251-291.

Van Andel T. H., 1973. Texture and dispersal of sediments in the Panama Basin, *J. Geol.*, **81**, 434-457.

Van Andel T. H., Von Herzen R. P., Phillips J. D., 1971. The Vema Fracture Zone and the tectonics of transverse shear zones in oceanic crustal plates, *Mar. Geophys. Res.*, **1**, 261-283.

Vangriesheim A., 1980. Antarctic bottom water flow through the Vema Fracture Zone, *Oceanol. Acta*, **3**, 2, 199-207.

Vergnaud-Grazzini C., 1978. Miocene and Pliocene oxygen and carbon isotopic changes at DSDP sites 372, 374 and 375: implications for pre-Messinian history of the Mediterranean, in: *Initial Reports of Deep-Sea Drilling Project*, **42**, edited by K. J. Hsü, L. Montadert *et al.*, part. I, Washington, US Gov. Print. Off., 829-836.

Vergnaud-Grazzini C., Pierre C., Letolle R., 1978. Paleoenvironment of the North-East Atlantic during the Cenozoic: oxygen and carbon isotope analyses at DSDP sites 398, 400 A and 401, *Oceanol. Acta*, **1**, 3, 381-390.

Von Rad U., 1970. Comparison between "magnetic" and sedimentary fabric in graded and cross laminated sand layers, Southern California, *Geol. Rundsch.*, **60**, 331-354.

Walker R. G., 1973. Mopping up the turbidite mess. A history of the turbidity current concept, in: *Evolving concepts in sedimentology*, edited by R. N. Ginsberg, Johns Hopkins Press. Baltimore, 1-37.

Wüst G., 1957. Stromgeschwindigkeiten und Strommengen in den tiefen des Atlantischen Ozeans, *Meteorwerk*, **6**, 2, 261-420.